Science Advances
AAAS

Supplementary Materials for

Targeting ABCA12-controlled ceramide homeostasis inhibits breast cancer stem cell function and chemoresistance

Jihong Cui *et al.*

Corresponding author: Wenjun Guo, wenjun.guo@einsteinmed.edu; Jihong Cui, jihong.cui@einsteinmed.edu

Sci. Adv. **9**, eadh1891 (2023)
DOI: 10.1126/sciadv.adh1891

The PDF file includes:

Other Supplementary Material for this manuscript includes the following:

Fig. S1.

Fig. S1: *SOX9* is expressed at heterogeneous levels in breast cancer cells.

A. T-SNE plots of scRNA-seq data (GSE75688) showing the distribution of cancer cells according to tumor samples (left, each color represents one tumor sample) and *SOX9* mRNA levels in individual cells (right, expression levels were represented by heat map). Data were analyzed by using CancerSEA (ExpID: EXP0053)

Fig. S2.

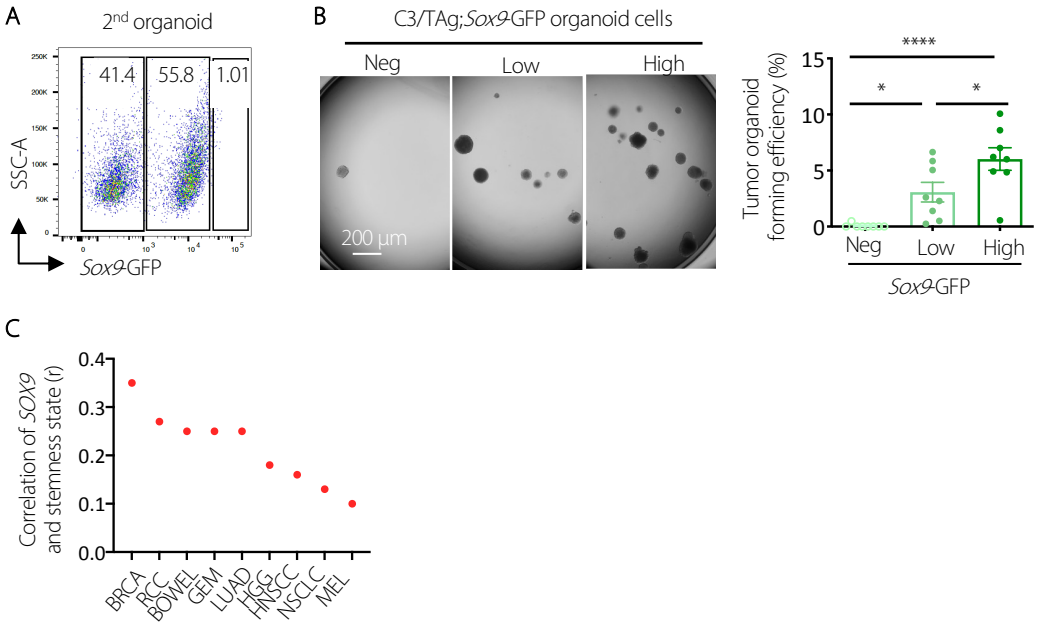

Fig. S2. SOX9^{high} cancer cells were enriched in tumorigenic potential.

A. Flow cytometry showing the distribution of *Sox9*-GFP^{neg}, ^{low} and ^{high} cells in tumor organoids generated from C3/TAg;*Sox9*-GFP^{high} tumor cells.
B. Representative images and quantification of organoid forming efficiency of *Sox9*-GFP^{neg}, ^{low} and ^{high} cells sorted from cultured *Sox9*-GFP;C3/Tag tumor organoids. Each dot represents one organoid line from a distinct tumor (n = 8).
C. Correlations between *SOX9* expression and the stemness score in different cancer types as determined by CancerSEA.

All data are represented as mean ± SEM. *P* values were determined by one-way ANOVA with Tukey's test (B). ****p < 0.0001; *p < 0.05.

Fig. S3.

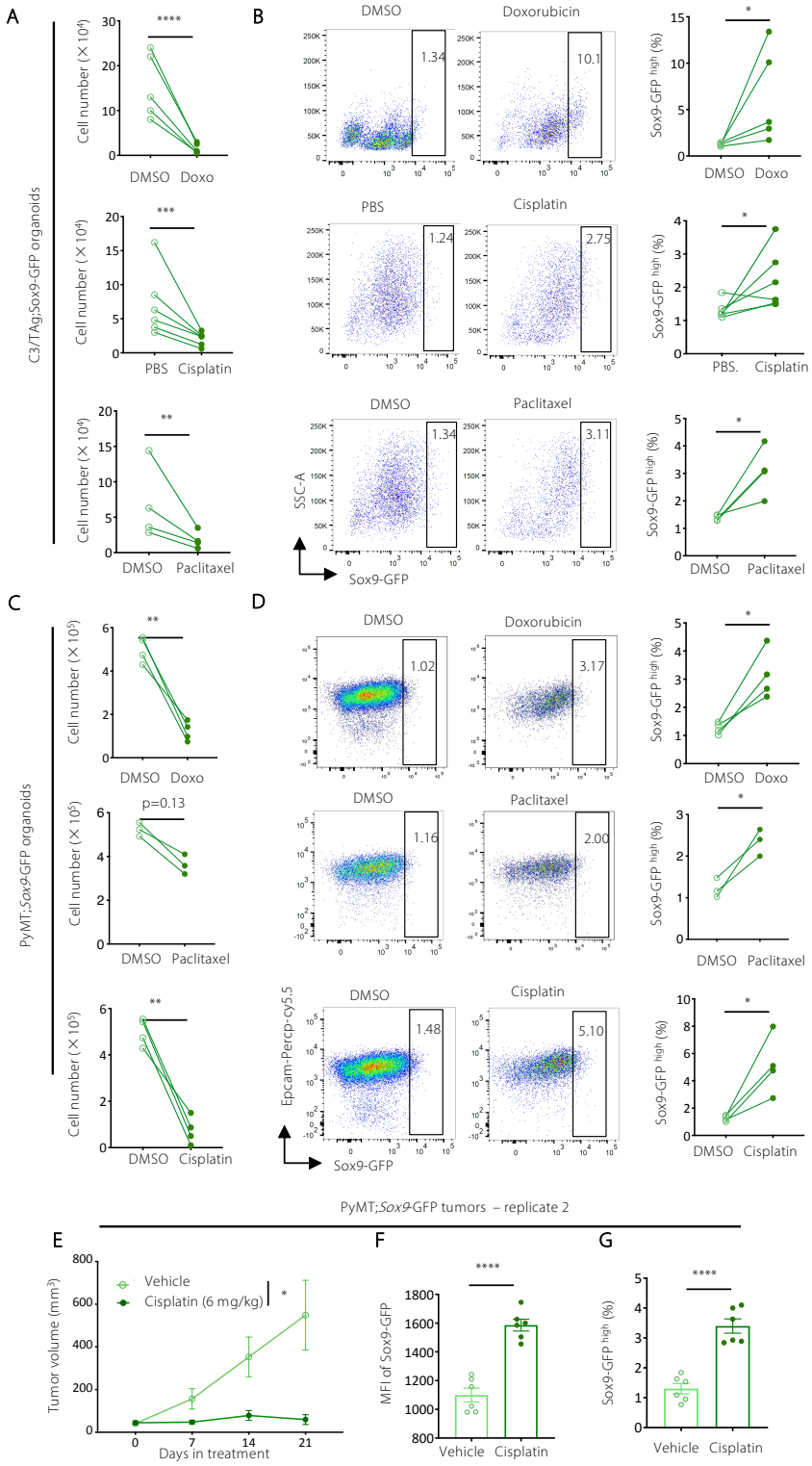
A
B
C
D
C3/TAg;Sox9-GFP organoids
PyMT;Sox9-GFP organoids
Cell number (X 10⁴)
Cell number (X 10⁵)
DMSO
Doxo
PBS
Cisplatin
Paclitaxel
Doxorubicin
p=0.13
SSC-A
Sox9-GFP
Epcam-Percp-cy5.5
Sox9-GFP high (%)
1.34
10.1
1.24
2.75
3.11
1.02
3.17
1.16
2.00
1.48
5.10
PyMT;Sox9-GFP tumors – replicate 2
E
F
G
Tumor volume (mm³)
Vehicle
Cisplatin (6 mg/kg)
Days in treatment
MFI of Sox9-GFP

Fig. S3. SOX9^{high} tumor cells are enriched after chemotherapy.

A. Effect of chemotherapeutic agents on tumor organoid cell numbers. Tumor organoids derived from different C3/TAg;*Sox9*-GFP tumors (n = 4-6) were treated with vehicle or various drugs (1 μM Doxorubicin (DOXO), 2 μM Cisplatin, or 5 nM Paclitaxel) for 3 days.

B. Flow cytometry measuring *Sox9*-GFP levels in tumor organoids as treated in (A). Top 1-2% of *Sox9*-GFP-expressing cells in the vehicle-treated group of the individual tumor were defined as the SOX9^{high} cells. The gating strategies for the chemotherapy treatment groups were based on their matching vehicle control of the same organoid line. The percentage of Sox9-GFP^{high} cells was quantified.

C. Effect of chemotherapeutic drugs on PyMT;Sox9-GFP tumor organoid growth. Tumor organoids derived from different tumors (n = 3-4) were treated with vehicle or chemotherapeutic drugs (1 μM Doxorubicin (Doxo), 5 nM Paclitaxel, or 2 μM Cisplatin) for 3 days.

D. Flow cytometry measuring *Sox9*-GFP levels in tumor organoids as treated in (C). Top 1-2% of *Sox9*-GFP-expressing cells in vehicle treated group of individual tumor lines were defined as the SOX9^{high} cells. The gating strategies for the chemotherapy treatment groups were based on their matching vehicle control of the same organoid line. Percentage of Sox9-GFP^{high} cells was quantified.

E. Effect of cisplatin on the growth of PyMT;*Sox9*-GFP tumors (replicate 2). 300,000 freshly isolated tumor cells from a spontaneous PyMT tumor were orthotopically injected into NOD/SCID mice. When tumors grew to approximately 3-5 mm in diameter, mice were treated with 6 mg/kg/week cisplatin or control for 3 weeks (Vehicle: n = 6; Cisplatin: n = 6).

F. The Sox9-GFP mean fluorescence intensity (MFI) of Lin-DAPI- tumor cells in tumors treated as in (E).

G. The percentage of SOX9^{high} cells in tumors treated as in (E).

All data are represented as mean ± SEM. P values were determined by paired two-tailed Student's t-test (A-D), two-way RM ANOVA (E), or unpaired two-tailed Student's t-test (F-G). ****p <0.0001; ***p <0.001; **p < 0.01; *p < 0.05.

Fig. S4

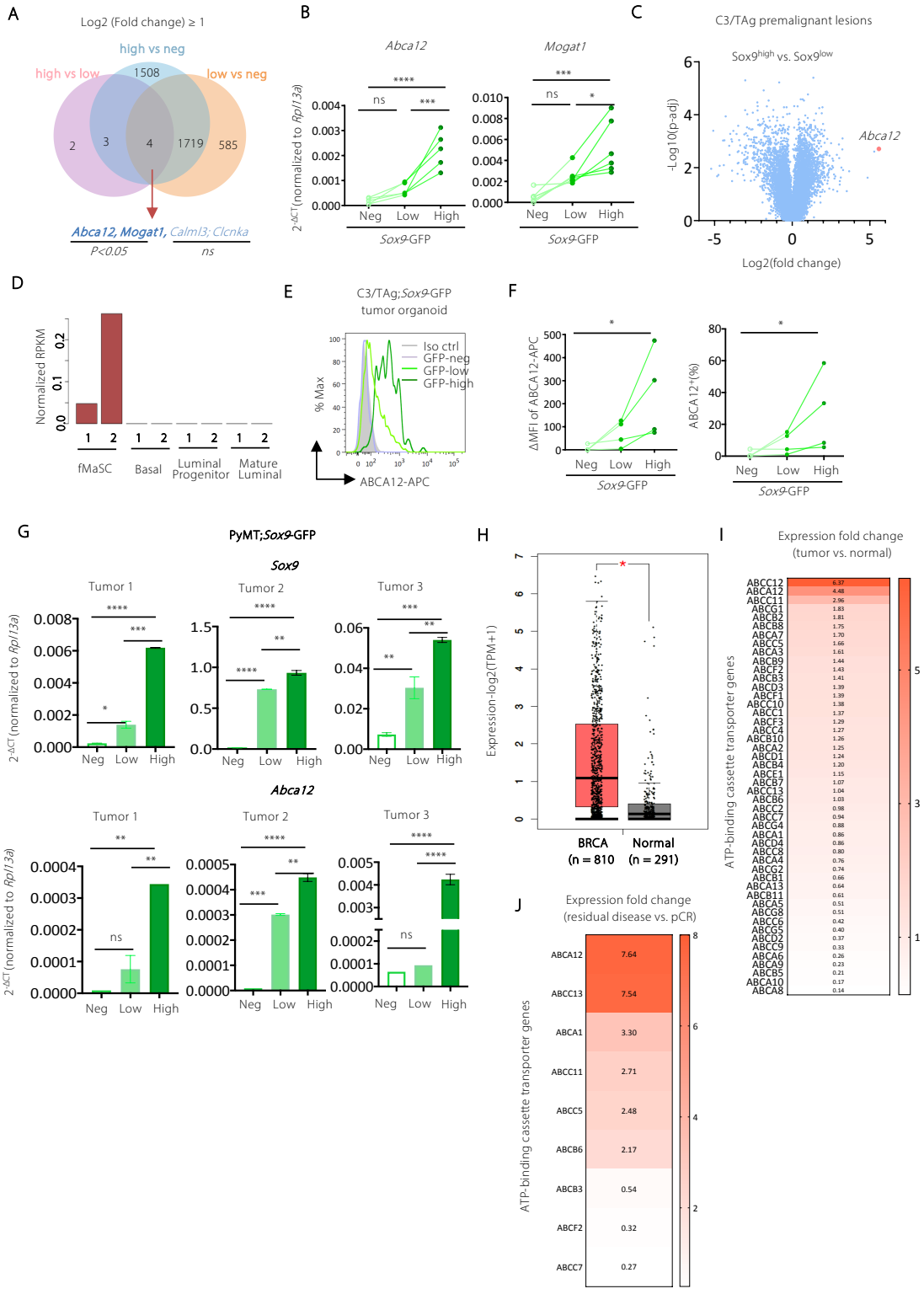
A
Log2 (Fold change) ≥ 1
high vs neg
high vs low
low vs neg
1508
2
3
4
1719
585
Abca12, Mogat1, Calml3; Clcnka
P<0.05
ns
B
Abca12
Mogat1
2-ΔCT (normalized to Rpl13a)
Neg Low High
Sox9-GFP
C
C3/TAg premalignant lesions
Sox9high vs. Sox9low
Abca12
-Log10(p-adj)
Log2(fold change)
D
Normalized RPKM
fMaSC
Basal
Luminal Progenitor
Mature Luminal
E
C3/TAg;Sox9-GFP tumor organoid
Iso ctrl
GFP-neg
GFP-low
GFP-high
% Max
ABCA12-APC
F
ΔMFI of ABCA12-APC
ABCA12+(%)
G
PyMT;Sox9-GFP
Sox9
Abca12
Tumor 1
Tumor 2
Tumor 3
H
Expression-log2(TPM+1)
BRCA (n = 810)
Normal (n = 291)
I
Expression fold change (tumor vs. normal)
ATP-binding cassette transporter genes
J
Expression fold change (residual disease vs. pCR)
ABCA12 7.64
ABCC13 7.54
ABCA1 3.30
ABCC11 2.71
ABCC5 2.48
ABCB6 2.17
ABCB3 0.54
ABCF2 0.32
ABCC7 0.27

Fig. S4. SOX9^{high} cancer stem cells upregulate the ABCA12 lipid transporter.

A. Venn diagram showing overlap of differentially expressed genes (Log2 (fold change) ≥ 1) between Sox9^{neg}, ^{low} and ^{high} C3/TAg tumor cells (n = 4 tumors).

B. qRT-PCR validation of candidate genes (*Abca12* and *Mogat1*) upregulated in SOX9^{high} C3/TAg tumor cells (n = 5).

C. Microarray comparing SOX9^{low} and ^{high} cells in C3/TAg premalignant lesions showing *Abca12* as the top upregulated gene in SOX9^{high} cells (GSE135892, n = 3 mice).

D. RNA-seq analysis of *Abca12* expression in fetal and adult mammary cell types. The graph was generated using https://wahl-lab-salk.shinyapps.io/Mammary_snATAC/ (Chung et al., 2019) (*35*). fMaSC, fetal mammary stem cell.

E. Flow cytometry measuring ABCA12 expression in SOX9^{neg}, ^{low} and ^{high} cells in C3/TAg;*Sox9*-GFP tumor organoids (n = 4).

F. Quantification of ABCA12 mean fluoresce intensity (MFI) and ABCA12^{+} populations in SOX9^{neg}, ^{low} and ^{high} cells in C3/TAg;*Sox9*-GFP tumor organoids by flow cytometry (n = 4).

G. *Sox9* and *Abca12* mRNA levels in sorted *Sox9*-GFP^{neg}, ^{low} and ^{high} PyMT tumor cells as determined by qRT-PCR. Three independent tumors were analyzed.

H. *ABCA12* expression in breast invasive carcinoma (BRCA) or normal mammary tissue. TPM, transcripts per million. (TCGA and GTEx data were analyzed by GEPIA2).

I. The expression levels of ATP-binding cassette transporter genes in breast cancer compared to normal tissue. Data were derived from Hlavac et al., 2013 (*38*).

J. The expression levels of ATP-binding cassette transporters in tumors that maintained residual disease and tumors that showed pathological complete response (pCR) after neoadjuvant chemotherapy (n=19 patients). The patients underwent sequential weekly paclitaxel / FEC (5-fluorouracil, epirubicin and cyclophosphamide) neoadjuvant chemotherapy. Data were extracted from published data in Park et al., 2006 (*39*).

All data are represented as mean ± SEM. *P* values were determined by one-way ANOVA with Turkey's test (B, G) or Dunn's test (F), or unpaired two-tailed Student's t-test (H). ****p <0.0001; ***p <0.001; **p < 0.01; *p < 0.05; ns, not significant.

Fig. S5

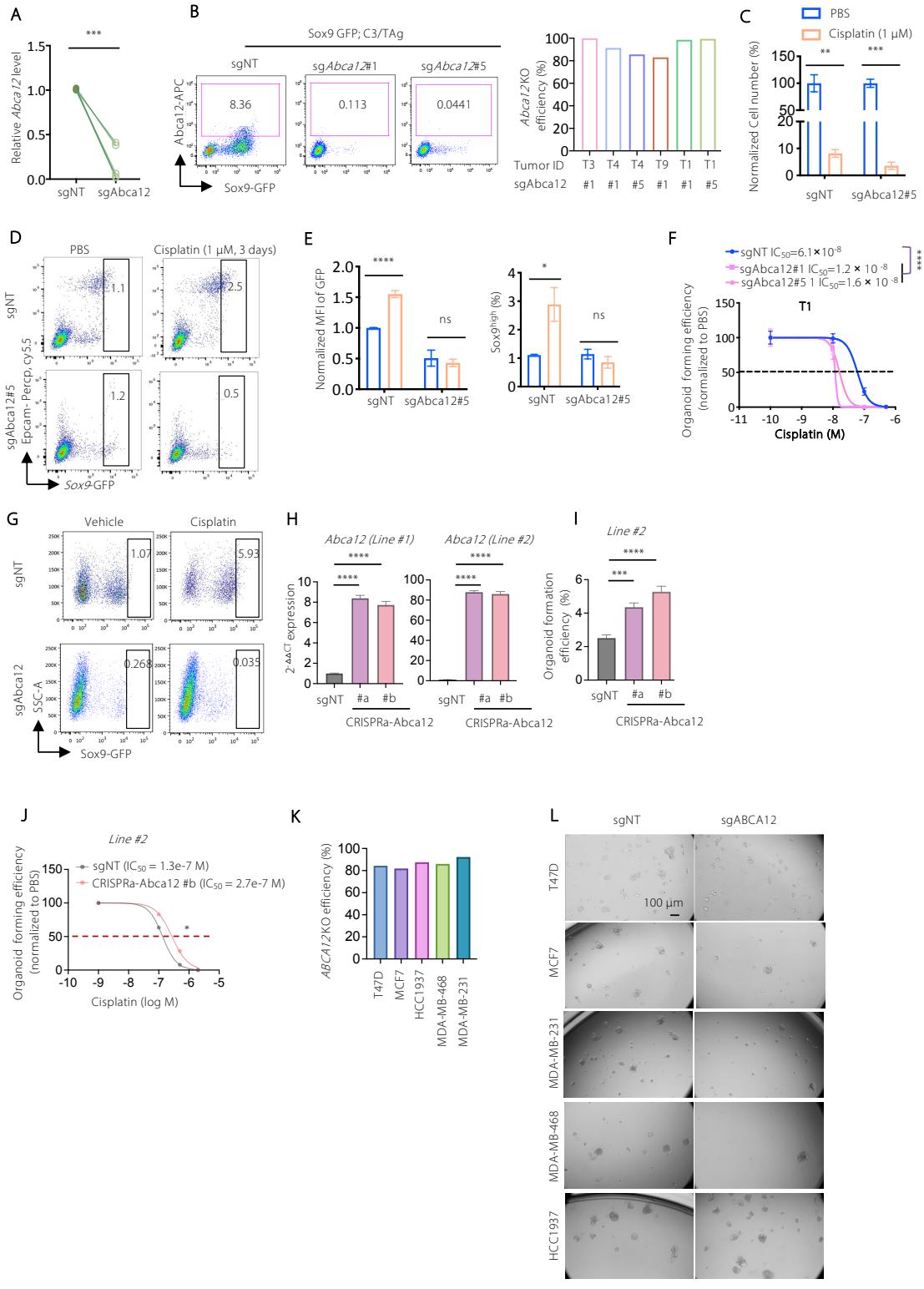
A
Relative Abca12 level
sgNT
sgAbca12
B
Sox9 GFP; C3/TAg
sgNT
sgAbca12#1
sgAbca12#5
8.36
0.113
0.0441
Abca12-APC
Sox9-GFP
Abca12KO efficiency (%)
Tumor ID T3 T4 T4 T9 T1 T1
sgAbca12 #1 #1 #5 #1 #1 #5
C
PBS
Cisplatin (1 μM)
Normalized Cell number (%)
sgNT
sgAbca12#5
D
PBS
Cisplatin (1 μM, 3 days)
sgNT
sgAbca12#5
1.1
2.5
1.2
0.5
Epcam- Percp. cy5.5
Sox9-GFP
E
Normalized MFI of GFP
Sox9high (%)
ns
sgNT
sgAbca12#5
F
sgNT IC50=6.1×10-8
sgAbca12#1 IC50=1.2 × 10 -8
sgAbca12#5 1 IC50=1.6 × 10 -8
T1
Organoid forming efficiency (normalized to PBS)
Cisplatin (M)
G
Vehicle
Cisplatin
sgNT
sgAbca12
1.07
5.93
0.268
0.035
SSC-A
Sox9-GFP
H
Abca12 (Line #1)
Abca12 (Line #2)
2-ΔΔCT expression
sgNT
#a
#b
CRISPRa-Abca12
I
Line #2
Organoid formation efficiency (%)
sgNT
#a
#b
CRISPRa-Abca12
J
Line #2
sgNT (IC50 = 1.3e-7 M)
CRISPRa-Abca12 #b (IC50 = 2.7e-7 M)
Organoid forming efficiency (normalized to PBS)
Cisplatin (log M)
K
ABCA12KO efficiency (%)
T47D
MCF7
HCC1937
MDA-MB-468
MDA-MB-231
L
sgNT
sgABCA12
100 μm
T47D
MCF7
MDA-MB-231
MDA-MB-468
HCC1937

Fig. S5. Downregulation of Abca12 impairs cancer stem cell activity and chemoresistance of SOX9^{high} cells.

A. Expression levels of *Abca12* mRNA in the sgNT or sgAbca12 C3/TAg;*Sox9*-GFP tumor organoids as determined by qRT-PCR. The significant reduction of *Abca12* mRNA levels was likely due to nonsense-mediated decay caused by frame-shifting indels introduced by CRISPR (n = 4).

B. Flow cytometry measuring ABCA12 deletion efficiency in C3/TAg;*Sox9*-GFP tumor organoids.

C. Relative cell numbers of sgNT and sgAbca12 C3/TAg; *Sox9*-GFP tumor organoids treated with vehicle or 1 μM cisplatin for 3 days (n = 3).

D. Flow cytometry measuring *Sox9*-GFP expression in sgNT and sgAbca12 C3/TAg;*Sox9*-GFP tumor organoids after being treated with vehicle or cisplatin for 3 days (n = 3).

E. Mean fluorescence intensity (MFI) of *Sox9*-GFP and percentage of *Sox9*-GFP^{high} cells in sgNT and sgAbca12 C3/TAg;*Sox9*-GFP tumor organoids after being treated with vehicle or cisplatin for 3 days, as measured in D.

F. Effect of cisplatin on tumor organoid forming efficiency of sgNT and sgAbca12 C3/TAg;*Sox9*-GFP cells (organoid line T1). 500 cells were seeded in medium containing different concentrations of cisplatin. Tumor organoids were counted after 5-day culture (n = 6).

G. Flow cytometry measuring *Sox9*-GFP expression in sgNT and sgAbca12 C3/TAg;*Sox9*-GFP tumors treated with vehicle or cisplatin for 3 weeks. Lin$^-$DAPI$^-$ cells were gated.

H. qRT-PCR quantifying the expression of *Abca12* in WT (sgNT) and Abca12 CRISPRa C3/TAg;*Sox9*-GFP tumor organoids.

I. Tumor organoid-forming efficiency of WT (sgNT) and Abca12 overexpression (CRISPRa-Abca12) C3/TAg;*Sox9*-GFP tumor cells (Line 2).

J. Effect of cisplatin on tumor organoid formation by WT (sgNT) and Abca12 overexpression (CRISPRa-*Abca12 #b*) C3/TAg;*Sox9*-GFP tumor organoids (n = 5, Line 2).

K. *ABCA12* deletion efficiency in human breast cancer cell lines measured by TIDE assay.

L. Representative images of tumor organoids formed by sgNT and sgABCA12-transduced breast cancer cell lines. 2,000 cells were seeded in organoid culture medium and tumor organoids were counted after 6-7 days.

All data are represented as mean ± SEM. P values were determined by paired (A) or unpaired two-tailed Student's t-test (C and E), one-way ANOVA with Dunnett's multiple comparisons test (H-I), Ordinary two-way ANOVA (F and J). ****p <0.0001; ***p <0.001; **p < 0.01; *p < 0.05; ns, not significant.

Fig. S6

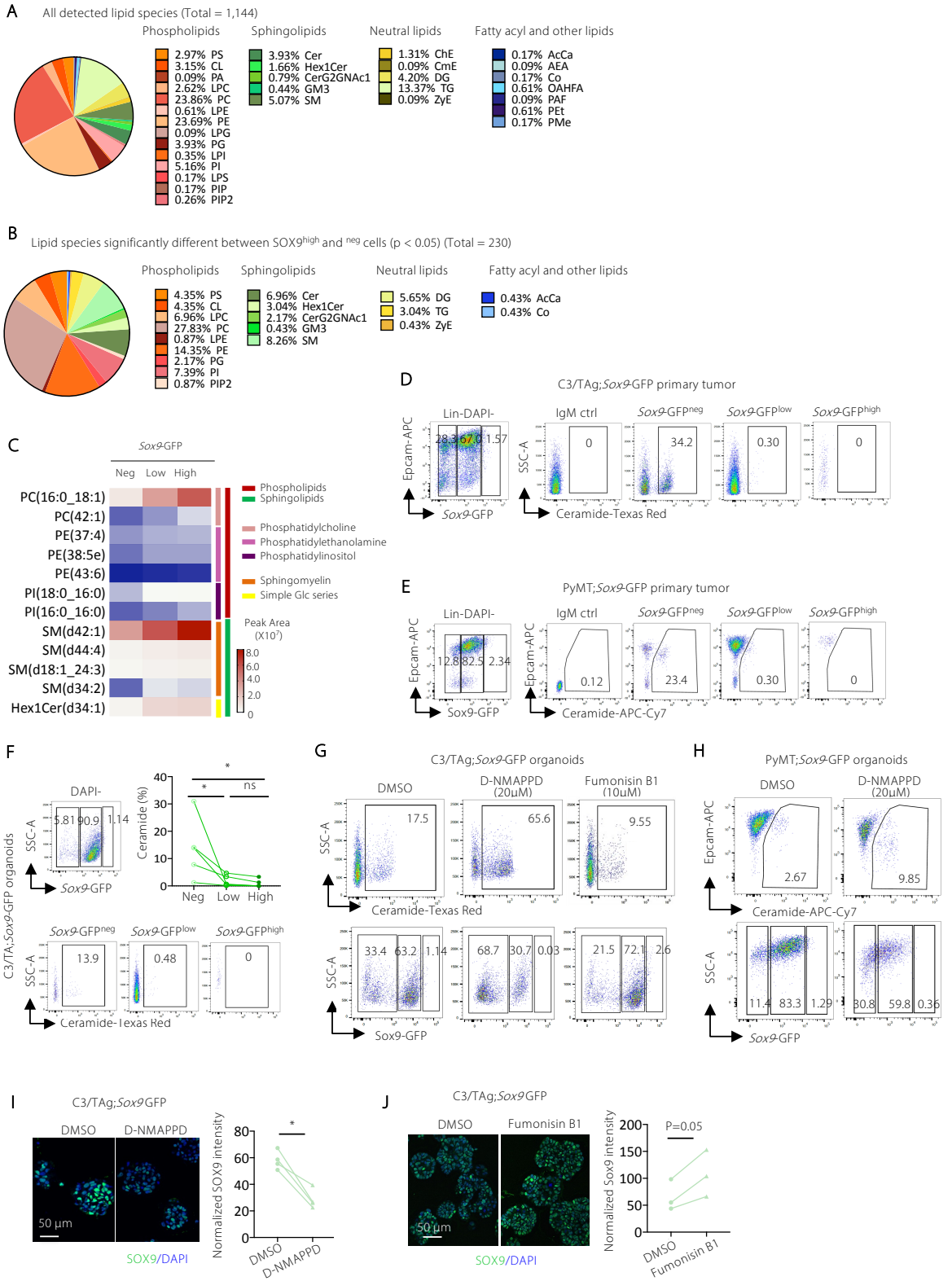
A
All detected lipid species (Total = 1,144)
Phospholipids
2.97% PS
3.15% CL
0.09% PA
2.62% LPC
23.86% PC
0.61% LPE
23.69% PE
0.09% LPG
3.93% PG
0.35% LPI
5.16% PI
0.17% LPS
0.17% PIP
0.26% PIP2
Sphingolipids
3.93% Cer
1.66% Hex1Cer
0.79% CerG2GNAc1
0.44% GM3
5.07% SM
Neutral lipids
1.31% ChE
0.09% CmE
4.20% DG
13.37% TG
0.09% ZyE
Fatty acyl and other lipids
0.17% AcCa
0.09% AEA
0.17% Co
0.61% OAHFA
0.09% PAF
0.61% PEt
0.17% PMe
B
Lipid species significantly different between SOX9high and neg cells (p < 0.05) (Total = 230)
Phospholipids
4.35% PS
4.35% CL
6.96% LPC
27.83% PC
0.87% LPE
14.35% PE
2.17% PG
7.39% PI
0.87% PIP2
Sphingolipids
6.96% Cer
3.04% Hex1Cer
2.17% CerG2GNAc1
0.43% GM3
8.26% SM
Neutral lipids
5.65% DG
3.04% TG
0.43% ZyE
Fatty acyl and other lipids
0.43% AcCa
0.43% Co
C
Sox9-GFP
Neg Low High
PC(16:0_18:1)
PC(42:1)
PE(37:4)
PE(38:5e)
PE(43:6)
PI(18:0_16:0)
PI(16:0_16:0)
SM(d42:1)
SM(d44:4)
SM(d18:1_24:3)
SM(d34:2)
Hex1Cer(d34:1)
Phospholipids
Sphingolipids
Phosphatidylcholine
Phosphatidylethanolamine
Phosphatidylinositol
Sphingomyelin
Simple Glc series
Peak Area (X10^7)
8.0
6.0
4.0
2.0
0
D
C3/TAg;Sox9-GFP primary tumor
Lin-DAPI-
IgM ctrl
Sox9-GFPneg
Sox9-GFPlow
Sox9-GFPhigh
Epcam-APC
Sox9-GFP
SSC-A
Ceramide-Texas Red
28.3 67.6 1.57
0
34.2
0.30
0
E
PyMT;Sox9-GFP primary tumor
Lin-DAPI-
IgM ctrl
Sox9-GFPneg
Sox9-GFPlow
Sox9-GFPhigh
Epcam-APC
Sox9-GFP
Ceramide-APC-Cy7
12.8 82.5 2.34
0.12
23.4
0.30
0
F
DAPI-
SSC-A
Sox9-GFP
5.81 90.9 1.14
Ceramide (%)
*
ns
Neg Low High
C3/TA;Sox9-GFP organoids
Sox9-GFPneg
Sox9-GFPlow
Sox9-GFPhigh
Ceramide-Texas Red
13.9
0.48
0
G
C3/TAg;Sox9-GFP organoids
DMSO
D-NMAPPD (20μM)
Fumonisin B1 (10uM)
SSC-A
Ceramide-Texas Red
17.5
65.6
9.55
Sox9-GFP
33.4 63.2 1.14
68.7 30.7 0.03
21.5 72.1 2.6
H
PyMT;Sox9-GFP organoids
DMSO
D-NMAPPD (20μM)
Epcam-APC
Ceramide-APC-Cy7
2.67
9.85
SSC-A
Sox9-GFP
11.4 83.3 1.29
30.8 59.8 0.36
I
C3/TAg;Sox9GFP
DMSO
D-NMAPPD
50 μm
SOX9/DAPI
Normalized SOX9 intensity
*
DMSO
D-NMAPPD
J
C3/TAg;Sox9GFP
DMSO
Fumonisin B1
50 μm
SOX9/DAPI
Normalized Sox9 intensity
P=0.05
DMSO
Fumonisin B1

Fig. S6. Lipidomic analyses uncovered that ABCA12 promotes SOX9 expression and cancer stemness by reducing ceramide abundance.

A. Lipid species identified by lipidomics profiling of $SOX9^{neg, low}$ and ^{high} tumor cells sorted from C3/TAg;*Sox9*-GFP tumors ($n = 5$).

B. The significantly altered lipid species between $SOX9^{high}$ and $SOX9^{neg}$ cells ($p < 0.05$).

C. Lipid species upregulated in $SOX9^{high}$ cells compared to $SOX9^{neg/low}$ cells ($p < 0.05$, $SOX9^{high}$ vs. $SOX9^{neg}$).

D. Flow cytometry measuring the levels of ceramide in $Sox9^{neg, low}$ and ^{high} C3/TAg primary tumor cells.

E. Flow cytometry measuring the levels of ceramide in $Sox9^{neg, low}$ and ^{high} PyMT primary tumor cells.

F. Flow cytometry measuring the levels of ceramide in C3/TAg tumor organoids.

G. *Sox9*-GFP and ceramide levels in C3/TAg tumor organoids treated with DMSO, D-NMAPPD (20μM) or Fumonisin B1 (10 μM) for 5 days, as measured by flow cytometry.

H. *Sox9*-GFP expression and ceramide levels in PyMT tumor organoids treated with DMSO or D-NMAPPD (10 μM) for 5 days, as measured by flow cytometry.

I. Representative immunofluorescence of SOX9 protein in C3/TAg tumor organoids treated with DMSO or D-NMAPPD (20 μM) for 3 days. Organoids were cultured without the drug for 2 days, and then treated for 3 days ($n = 4$).

J. Representative immunofluorescence of SOX9 protein in C3/TAg tumor organoids treated with DMSO or Fumonisin B1 (10 μM) for 5 days.

All data are represented as mean ± SEM. *P* values were determined by one-way ANOVA with Holm-Šídák's multiple comparisons test (F) or paired two-tailed Student's t-test (I-J). *$p < 0.05$; ns, not significant.

Fig. S7

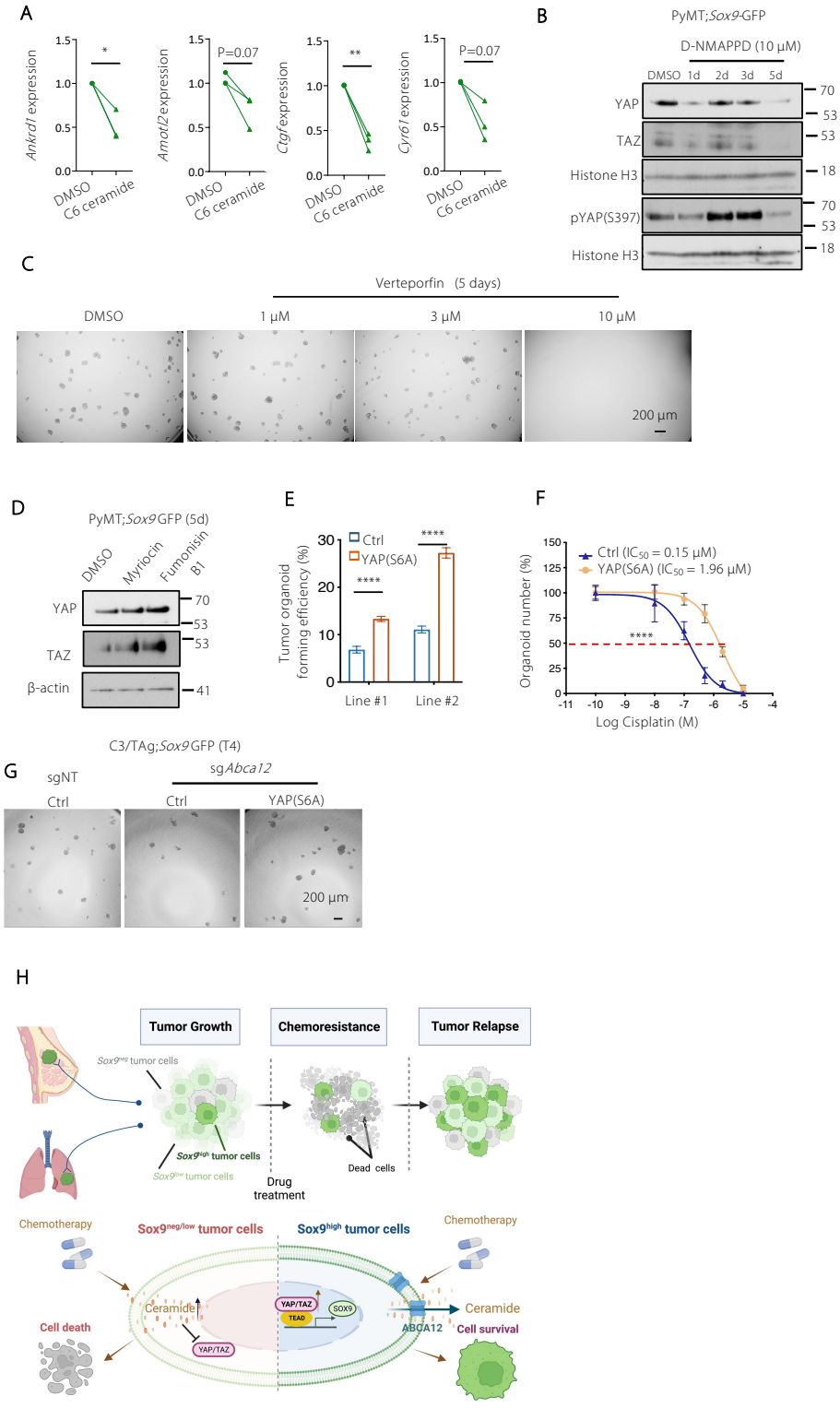
A
Ankrd1 expression
Amotl2 expression
Ctgf expression
Cyr61 expression
DMSO
C6 ceramide
P=0.07
B
PyMT;Sox9-GFP
D-NMAPPD (10 μM)
DMSO 1d 2d 3d 5d
YAP
TAZ
Histone H3
pYAP(S397)
C
Verteporfin (5 days)
DMSO
1 μM
3 μM
10 μM
200 μm
D
PyMT;Sox9GFP (5d)
DMSO
Myriocin
Fumonisin B1
β-actin
E
Tumor organoid forming efficiency (%)
Ctrl
YAP(S6A)
Line #1
Line #2
F
Organoid number (%)
Ctrl (IC50 = 0.15 μM)
YAP(S6A) (IC50 = 1.96 μM)
Log Cisplatin (M)
G
C3/TAg;Sox9GFP (T4)
sgNT
sgAbca12
Ctrl
YAP(S6A)
200 μm
H
Tumor Growth
Chemoresistance
Tumor Relapse
Sox9neg tumor cells
Sox9high tumor cells
Sox9low tumor cells
Dead cells
Drug treatment
Chemotherapy
Sox9neg/low tumor cells
Sox9high tumor cells
Ceramide
Cell death
YAP/TAZ
TEAD
SOX9
ABCA12
Cell survival

Fig. S7: Ceramide suppressed SOX9 expression via inhibition of the YAP/TAZ pathway.

A. qRT-PCR quantifying the expression of the indicated genes in C3/TAg tumor organoids after treatment with DMSO or C6-ceramide (10 μM) for 3 days (n = 3).

B. Western blot showing the effect of D-NMAPPD (10 μM) on YAP, pYAP(S397), and TAZ levels in PyMT tumor organoids (two independent experiments were performed).

C. Effect of verteporfin (1, 3, 10 μM) on organoid forming efficiency of C3/TAg tumor cells (n = 3).

D. Western blot showing the effect of Myriocin (2 μM) or Fumonisin B1 (10 μM) on YAP and TAZ levels in PyMT tumor organoids (n = 2).

E. Effect of YAP activation (YAP1 (S6A)) on organoid forming efficiency of C3/TAg tumor cells. Two tumor lines are used.

F. Effect of cisplatin on organoid forming efficiency of control and YAP1 (S6A)-expressing C3/TAg tumor cells. Cells were treated with vehicle or cisplatin for 5 days. The relative numbers of organoids were normalized to the vehicle control.

G. Effect of YAP1 (S6A) expression on organoid forming efficiency by sgNT1 and sg*Abca12* C3/TAg tumor cells.

H. A proposed model of the impact of the ABCA12-ceramide-YAP/TAZ-SOX9 axis on tumor heterogeneity and drug resistance (generated by BioRender).

All data are represented as mean ± SEM. *P* values were determined by paired (A) or unpaired (E) two-tailed Student's t-test, or two-way ANOVA (F). ****p <0.0001; **p < 0.01; *p < 0.05.

Table S1.

	Forward	Reverse
Rpl13a	CCTGCTGCTCTCAAGGTTGTT	TGGTTGTCACTGCCTGGTACTT
SV40	CCAATTATGTCACACCAC AGA	TTGCTGTCGTTACTGAGGATG
EGFP	CTACCCCGACCACATGAA	TCTTGTAGTTGCCGTCGTCC
Abca12	TCCTGGTGTGGAAAAATTGGC	GTGCGAGGTAACAAGTTGGTT
Sox9	AGGAAGCTGGCAGACCAGTA	CGTTCTTCACCGACTTCCTC
Mogat1	TGGTGCCAGTTTGGTTCCAG	TGCTCTGAGGTCGGGTTCA
Cyr61	CTGCGCTAAACAACTCAA	GCAGATCCCTTTCAGAGCGC
Ankrd1	GCTGGTAACAGGCAAAAAGA AC	CCTCTCGCAGTTTCTCGCT
Amotl2	GGAGAAGAGTTGCCCACCTAT	TCGAAGAGCTTCATCCTGTCG
Ctgf	GGGCCTCTTCTGCGATTTC	ATCCAGGCAAGTGCATTGGTA

Table S1. qRT-PCR primers

Data S1: Supplementary information: western blot scans

Fig. 1B: Sox9

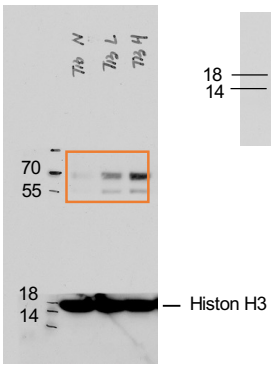

Fig. 1B: Histone H3

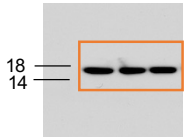

Western blot scanned films. Boxes indicate lanes shown in the figures.

Supplementary information: western blot scans

Fig. 5J: Sox9

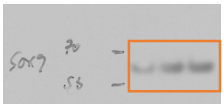

Fig. 5J: β-actin

Western blot scanned films. Boxes indicate lanes shown in the figures.

Supplementary information: western blot scans

Fig. 7C:

C3/TAg;*Sox9* GFP : SOX9

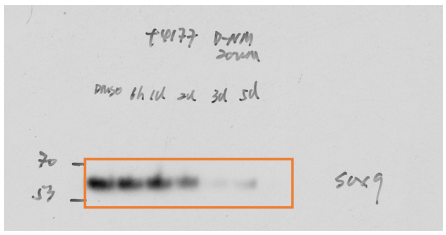

C3/TAg;*Sox9* GFP : β-actin

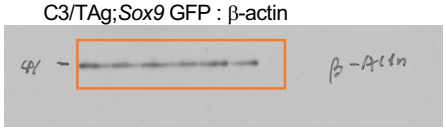

Fig. 7C:

PyMT;*Sox9* GFP

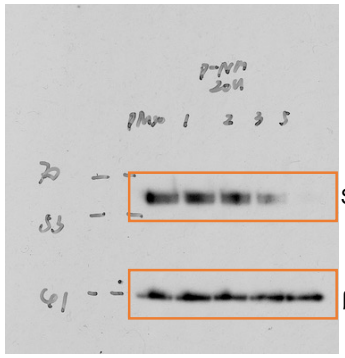

Fig. 7E:

C3/TAg;*Sox9* GFP : YAP

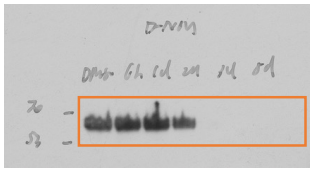

C3/TAg;*Sox9* GFP : TAZ

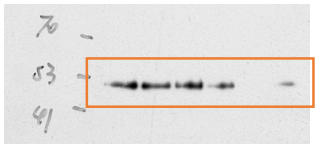

C3/TAg;*Sox9* GFP : β-actin

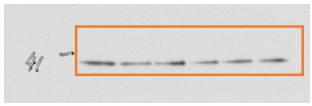

Fig. 7H:

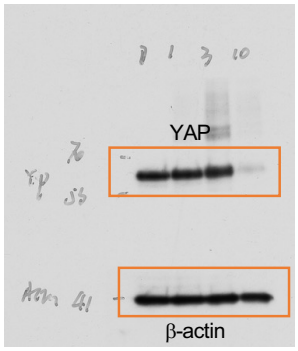

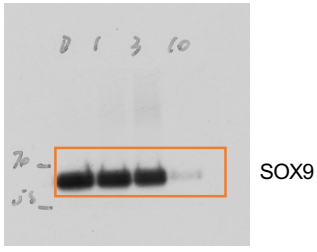

Fig. 7K:

C3/TAg;*Sox9* GFP : SOX9

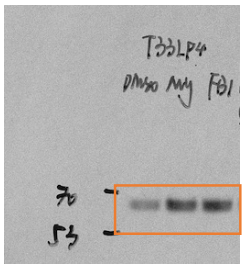

Histione H3

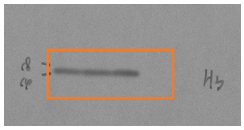

PyMT;*Sox9* GFP : SOX9

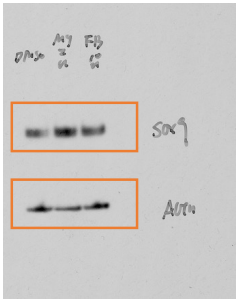

Fig. 7N:

YAP

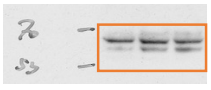

Histone H3

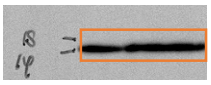

β-actin

41

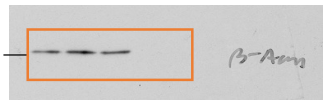

TAZ

53

Fig. 7O:

YAP

SOX9

β-actin

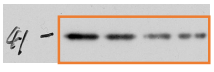

Fig. 7P:

YAP

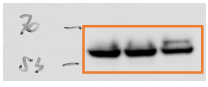

SOX9

70

53

β-actin

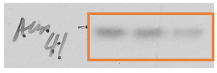

Western blot scanned films. Boxes indicate lanes shown in the figures.

Supplementary information: western blot scans

Fig. S7B:

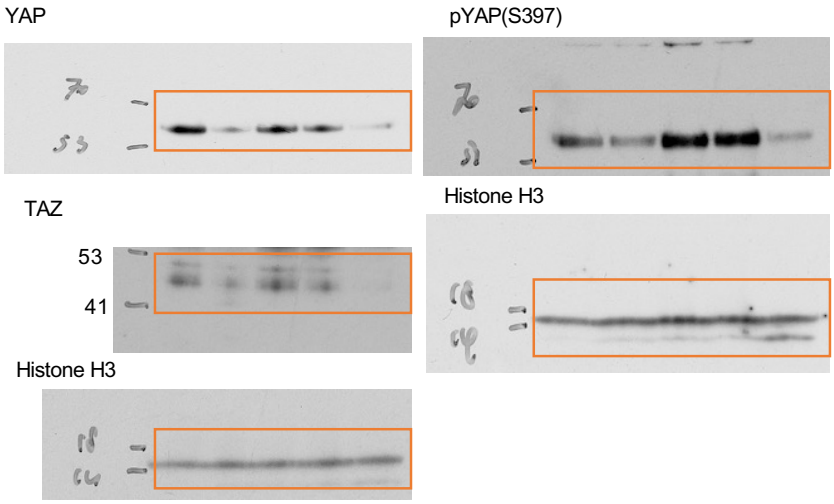

Fig. S7D:

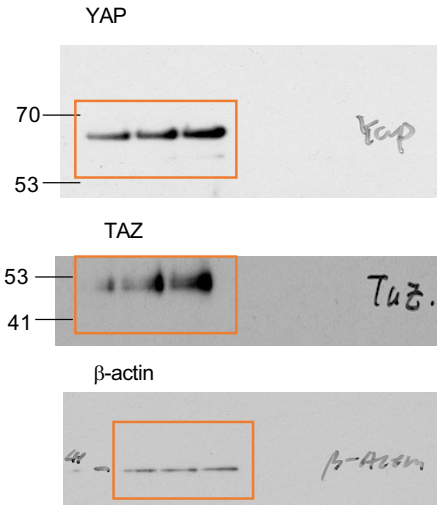

Western blot scanned films. Boxes indicate lanes shown in the figures.

Data S2: KEY RESOURCES TABLE

REAGENT or RESOURCE	SOURCE	IDENTIFIER
Antibodies		
Biotin anti-mouse TER-119	BioLegend	Cat#116204
Biotin anti-mouse CD45	BioLegend	Cat#103104
Biotin anti-mouse CD31	BioLegend	Cat#102404
APC anti-mouse CD326 (Ep-CAM)	BioLegend	Cat#118214
PerCP/Cy5.5 anti-mouse CD326 (Ep-CAM)	BioLgend	Cat#118220
Streptavidin V450	BD Biosciences	Cat#560797
Goat-anti-ABCA12	Novus Biologicals	Cat#NB100-93466
Rabbit anti-human ABCA12	Sigma Aldrich	Cat#HPA043194
Mouse anti-ceramide	Sigma-Aldrich	Cat#C8104
Rabbit anti-Yap	Cell Signaling Technology	Cat#14074S
Rat anti-Keratin 8	Developmental Studies Hybridoma Bank	Cat#TROMA-I
Rabbit anti-Keratin 14	BioLegend	Cat#905304
Chicken anti-Keratin 14	BioLegend	Cat#906004
Rabbit anti-Phospho-YAP (Ser397)	Cell Signaling Technology	Cat#13619S
Rabbit anti-Taz	Cell Signaling Technology	Cat#72804S
Mouse anti-β-actin	BD Biosciences	Cat#612656
Mouse anti-Histone H3	Cell Signaling Technology	Cat#14269S
Rabbit anti-V5-Tag (D3H8Q)	Cell Signaling Technology	Cat#13202S
Goat IgG Isotype Control	Novus Biologicals	Cat#NB410-28088
Goat anti-Chicken IgY (H+L) Secondary Antibody, Alexa Fluor 488	Invitrogen	Cat#A-11039
Goat anti Chicken IgY (H+L) Secondary Antibody, Alexa Fluor 633	Invitrogen	Cat#A-21103
Alexa Fluor 488-AffiniPure Goat Anti-Rabbit IgG (H+L)	Jackson ImmunoResearch	Cat#111-545-003
Goat anti-Rabbit IgG (H+L) Cross-Adsorbed Secondary Antibody, Alexa Fluor 568	Invitrogen	Cat#A-11011
Alexa Fluor 647-conjugated AffiniPure Goat Anti-Rabbit IgG (H+L)	Jackson ImmunoResearch	Cat#111-605-144
Alexa Fluor 488-AffiniPure Goat Anti-Rat IgG (H+L)	Jackson ImmunoResearch	Cat#112-545-143
Alexa Fluor 647-AffiniPure Goat Anti-Rat IgG (H+L)	Jackson ImmunoResearch	112-605-143
Goat anti-Rat IgG (H+L) Secondary Antibody, Alexa Fluor® 568 conjugate	Invitrogen	Cat#A-11077
Alexa Fluor 647 donkey anti-goat IgG (H+L)	Invitrogen	Cat#A21447
Anti-IgM, k Isotype Ctrl Mouse Monoclonal Antibody	BioLegend	Cat#401602

Goat anti Mouse IgM Cross Adsorbed Secondary Antibody, DyLight 755	Invitrogen	Cat#SA5-10155
Goat anti-Mouse IgM Cross Adsorbed Secondary Antibody, DyLight 594,	Invitrogen	Cat#SA5-10152
ImmPRESS HRP Anti-Rabbit Ig (Peroxidase) Polymer Detection Kit	Vector Laboratories	Cat#MP-7401
ImmPRESS HRP Anti-Goat Ig (Peroxidase) Polymer Detection Kit	Vector Laboratories	Cat#MP-7405
HRP Donkey anti-rabbit IgG	BioLegend	Cat#406401
HRP Goat anti-mouse IgG	BioLegend	Cat#405306
Bacterial and virus strains		
ElectroMAX Stbl4 Competent Cells	Life Technologies	Cat#1635018
NEB® Stable Competent E. coli (High Efficiency)	New England Biolabs	Cat#C3040I
Biological samples		
Patient-derived xenografts (PDX)	ref. 33	N/A
Mouse tumor tissue	This paper	N/A
Chemicals, peptides, and recombinant proteins		
Advanced DMEM/F12	Gibco	Cat#12634028
DMEM/Hams F-12 50/50 Mix	Corning	Cat#10-092-CV
DMEM	Corning	Cat#10-017-CV
Epicult (R) - B Mouse Medium Kit	STEMCELL Technologies	Cat#05610
Fetal Bovine Serum	VWR	Cat# 97068-085
HyClone Calf Serum, U.S. origin	Cytiva	Cat#SH30073.03
GlutaMAX™ Supplement 100x	Gibco	Cat#35050061
Penicillin-streptomycin 100x	Corning	Cat# 30-002-CI
PBS, 1X without calcium and magnesium	Corning	Cat#21-040-CV
Trypan Blue solution, 0.4%	Corning	Cat#25900CI
Bovine Serum Albumin, Heat Shock Treated (BSA)	Fisher Scientific	Cat# BP1600100
Poly(2-hydroxyethyl methacrylate)	Sigma-Aldrich	Cat#P3932
Ethanol 200 Proof	Becon Labs	Cat#2701
Collagenase, Type III	Worthington Biochemical	Cat# LS004182
Deoxyribonuclease I (DNase I)	Worthington Biochemical; Roche	Cat# LS002139; Cat#104159
Neutral Protease (Dispase)	Worthington Biochemical	Cat# LS02109
Trypsin 0.05% with 0.53 mM EDTA	Corning	Cat# 25-052-CI
Epidermal Growth Factor human (EGF)	Sigma-Aldrich	Cat#E9644
Fibroblast Growth Factor basic Protein, Human recombinant (FGF2)	Millpore-Sigma	Cat#GF003
Heparin sodium salt, from porcine intestinal mucosa	Millpore-Sigma	Cat#H3149
Y-27632 (hydrochloride), ROCK inhibitor	Cayman Chemical Company	Cat#10005583

Hyaluronidase	Worthington Biochemical	Cat# LS002592
Matrigel Basement Membrane Matrix	Corning	Cat#354234
Dimethylsulfoxide (DMSO)	Millpore-Sigma	Cat#MX-1458
Red blood cell lysing buffer	Sigma-Aldrich	Cat#R7757
Agarose, Low Melting Point	Promega	Cat#V2111
32% Paraformaldehyde (formaldehyde) aqueous	Electron Microscopy Sciences	Cat#15714S
Xylene	Fisher Chemical	Cat# BPX3P1GAL
DAPI Fluoromount-G mounting medium	Southernbiotech	Cat#0100-20
Antigen Unmasking Solution, Citric Acid Based	Vector Laboratories	Cat#H3300
Retriever for Antigen Unmasking	Electron Microscopy Sciences	Cat#62700-10
UltraPureTM 0.5M EDTA, pH 8.0	ThermoFisher	Cat#15575020
Halt™ Protease Inhibitor Cocktails	Fisher Scientific	Cat#PI87786
Fisher Chemical™ Permount™ Mounting Medium	Fisher Scientific	Cat#SP15100
Methanol	EMD Millipore	Cat#MX0488-1
30% Hydrogen Peroxide	Sigma-Aldrich	Cat#31642
Lenti-X Concentrator	Clontech Laboratories	Cat#631232
Polybrene	EMD Millipore	Cat#TR-1003-G
Blasticidin S HCl	Corning	Cat#MT30100RB
Puromycin dihydrochloride	Tocris	Cat#4089
DAPI	Sigma-Aldrich	Cat# D8417
C6-ceramide	Cayman Chemical Company	Cat#62525
D-NMAPPD	Cayman Chemical Company	Cat#10006305
Myriocin	Cayman Chemical Company	Cat#63150
D-NMAPPD; ≥98% (HPLC) (*In vivo* treatment)	Sigma-Aldrich	Cat#SML2358
Fumonisin B1	Cayman Chemical Company	Cat#62580
Cisplatin	Cayman Chemical Company	Cat#13119
Doxorubicin	LC Laboratories	Cat#D-4000
Paclitaxel	LC Laboratories	Cat#P-9600
Kolliphor EL	Sigma-Aldrich	Cat#C5135
BLUEstain™ Protein ladder	Goldbio	Cat#P007-3000
Rat-tail collagen I	Corning	Cat#354236
Tris-HCl Buffer 1M, pH 7.5, Sterile	Bioworld	Cat# 42020268-3
Sodium Chloride	Fisher Scientific	Cat# BP358212
Sodium deoxycholate	Sigma-Aldrich	Cat# 30970
Sodium Dodecyl Sulfate	Fisher Scientific	Cat#BP-166
Nonidet P-40 Substitute	IBI Scientific	Cat#IB01140
10% Formalin	Fisher Scientific	Cat#SF98-4
NuPAGE® LDS Sample Buffer (4X)	Invitrogen	Cat#NP0007

NuPAGE® MOPS SDS Running Buffer (for Bis-Tris Gels only) (20X)	Invitrogen	Cat#NP0001
NuPAGE® Transfer Buffer (20X)	Invitrogen	Cat#NP00061
Fisher Healthcare Tissue-Plus OCT Compound	Fisher Scientific (FS)	Cat#23730571
Carnation Instant Nonfat Dry Milk	Amazon	Cat#B07NQDB3XS
Carbenicillin (Disodium)	Goldbio	Cat#C-103-5
MEM Non-Essential Amino Acids Solution 100mM (100X)	Invitrogen	Cat#11140-050
MEM Sodium Pyruvate Solution 100mM (100X)	Invitrogen	Cat#11360-070
Western Blot Stripping buffer	Thermo Fisher Scientific	Cat#46430
ScaI-HF - 5,000 units	New England Biolabs	Cat#R3122L
Esp3I (BsmBI)	New England Biolabs	Cat#R0734S
T4 DNA Ligase	New England Biolabs	Cat#M0202S
BamHI-HF® Restriction Enzyme, 20,000 units/ml, 10,000 units	New England Biolabs	Cat#R3136S
Jetprime transfection reagent	VWR	Cat#89129-924
BSA fraction V	Fisher Scientific	Cat#BP1600100
Isopropanol	Fisher Scientific	Cat#BP26184
2-Mercaptoethanol	Sigma-Aldrich	Cat#M314825ML
Tween 20, molecular biology grade	Sigma-Aldrich	Cat#P9416
Triton-X100	Sigma-Aldrich	Cat#X100
Critical commercial assays		
Western Lightning ECL Pro	PerkinElmer Health Sciences	Cat#NEL121001EA
DAB Peroxidase (HRP) Substrate Kit, 3,3′-diaminobenzidine	Vector Laboratories	Cat#SK-4100
High-Capacity cDNA Reverse Transcription Kit	Applied Biosystems	Cat#4368814
Power SYBR® Green PCR Master Mix	Applied Biosystems	Cat#4368708
PrimeSTAR MAX DNA polymerase	Takara Bio	Cat#R045A
NEBuilder® HiFi DNA Assembly Master Mix	New England Biolabs	Cat#E2621S
Qubit® RNA HS Assay Kit	Thermo Fisher Scientific	Cat#Q32852
Dura Chemiluminescent Substrate	Fisher Scientific	Cat#PIA34075
Quick-RNA Purification Kit, Microprep	Zymo Research	Cat#R1050
RNeasy Plus Micro Kit	Qiagen	Cat#74034
Direct-zol™ RNA MiniPrep	Zymo Research	Cat#R2072
NEBNext Ultra II Directional library prep kit	New England Biolabs	Cat#E7765
NucleoSpin® Gel and PCR Clean-Up	Takara	Cat#740609
ZymoPURE II Plasmid Maxiprep Kit	Zymo Research	Cat#D4203
Zyppy™ Plasmid Miniprep Kit	Zymo Research	Cat#D4020

NEB 10-beta/Stable Outgrowth Medium	New England Biolabs (NEB)	Cat#B9035S
Quick Ligation Kit	New England Biolabs (NEB)	Cat#M2200S
SapphireAmp® Fast PCR Master Mix	Clontech	Cat#RR350B
Experimental models: Cell lines		
HEK293T	ATCC	CVCL_0063
Tumor organoid	This paper	N/A
Experimental models: Organisms/strains		
Mouse: FVB-Tg(C3-1-TAg)cJeg/JegJ; FVBJ.B6(Cg) Tg(Sox9-EGFP)EB209Gsat/Mmucd	ref. 26	N/A
Mouse: Sox9-GFP; RFP; MMTV-PyMT	This paper	N/A
Mouse: CAG::mRFP1	The Jackson Laboratory	Cat #005884
Mouse FVB/N-Tg(MMTV-PyVT)634Mul/J	The Jackson Laboratory	Cat #002374
Mouse: NOD/SICD	The Jackson Laboratory	Cat #001303
Mouse: NSG	The Jackson Laboratory	Cat #005557
Oligonucleotides		
Primers for RT-PCR are found in the RT-PCR primers table	This paper	NA
Primers for cloning are found in the Method details	This paper	NA
Primers for C3/TAg genotyping: 5'- CAG AGC AGA ATT GTG GAG TGG; 5'-GGA CAA ACC ACA ACT AGA ATG CAG TG	This paper	NA
Primers for PyMT genotyping: 5'- GGA AGC AAG TAC TTC ACA AGG G 5'- GGA AAG TCA CTA GGA GCA GGG	This paper	NA
Primer for genotyping internal control: 5'- CAA ATG TTG CTT GTC TGG TG; 5'- GTC AGT CGA GTG CAC AGT TT	This paper	NA
Recombinant DNA		
pLVX-Puro	Takara	Cat#632164
pLVX-Puro-SOX9	This paper	N/A
pMD2.G	Addgene	Cat#Addgene_12259
pCMVR8.74	Addgene	Cat#Addgene_22036
LentiCRISPRv2 puro	Addgene	Cat#Addgene_98290
LentiCRISPRv2 puro-sgNT	This paper	N/A
LentiCRISPRv2 puro-sgAbca12 (mouse)	This paper	N/A
LentiCRISPRv2 puro-sgABCA12 (human)	This paper	N/A
Lenti-EF1a-dCas9-VPR-Puro	Addgene	Cat#Addgene_99373

pLKO5.sgNT.EFS.tRFP	This paper	N/A
pLKO5.sgAbca12.EFS.tRFP	This paper	N/A
pLX304	Addgene	Cat#Addgene_25890
pLX304-YAP1(S6A)-V5	Addgene	Cat#Addgene_42562
Software and algorithms		
Image J	National Institutes of Health and the Laboratory for Optical and Computational Instrumentation	https://imagej.nih.gov/ij/
QuPath	The university of Edinburgh	https://qupath.github.io/
GSEA4.0.2	NCI	https://www.gsea-msigdb.org/gsea/index.jsp
Slide Book software 6.0	3i-intelligent imaging	https://www.intelligent-imaging.com/slidebook
CaseViewer	3D HISTECH	https://www.3dhistech.com/solutions/caseviewer/
Graphpad Prism 8 and 9	Graphpad	https://www.graphpad.com/
Hisat2	ref. 68	http://daehwankimlab.github.io/hisat2/
Stringtie	ref. 69	http://ccb.jhu.edu/software/stringtie/index.shtml?t=manual
FastQC (version 0.64)	Babraham Bioinformatics	https://www.bioinformatics.babraham.ac.uk/projects/fastqc/
DeSeq2 (1.34.0)	ref. 70	http://bioconductor.org/packages/DESeq2/
Galaxy	Galaxy	https://usegalaxy.org/
BD FACSDiva 6.1	BD Biosciences	Cat#643629
FlowJo 9.3.2 and 10.4.0	FlowJo, LLC	https://www.flowjo.com/solutions/flowjo/downloads/
Gen5 (Bioteck)	Agilent	https://www.biotek.com/products/software-robotics-software/gen5-microplate-reader-and-imager-software/
QuantStudio 6 Real-Time PCR Software	Applied Biosystem	https://www.thermofisher.com/us/en/home/global/forms/life-science/quantstudio-6-7-flex-software.html
LIPEA	Biomedical Cybernetics Group.	https://lipea.biotec.tu-dresden.de/home
Other		
24-well Transwell cell	Greiner Bio-One	662638
Nunc® Lab-Tek™ II Chamber Slide	Thermo Scientific	154534PK
Super Pap Pen	Electron Microscopy Sciences	71312
Cell Scrapers	Biologix Research Company	70-1180
1mm electroporation Cuvettes	Thermo Fisher Scientific	FB101
NuPAGE™ Novex™ 4-12% Bis-Tris Protein Gels, 1.0 mm, 12-well	Thermo Fisher	NP0322BOX
FILM, HYBLOT, HGH SENSITIVITY 5x7"	Thomas Scientific	1156P38
Millipore* Immobilon* PVDF Transfer Membranes	Thermo Fisher Scientific	IPVH00010
0.22 µm pore size sterile syringe filter	Foxx Life Sciences	Cat# 371-2215-OEM
Cell strainer, 40 µm	Fisher Scientific	Cat# 22-363-547

Whatman Puradisc 25 mm Polyethersulfone Syringe Filter, 0.45 µm, sterile	Cytiva	Cat#6780-2504

Data S3. (separate file)
Source Data